Supplementary Information (SI) for Journal of Materials Chemistry A.
This journal is © The Royal Society of Chemistry 2026

Supplementary Materials

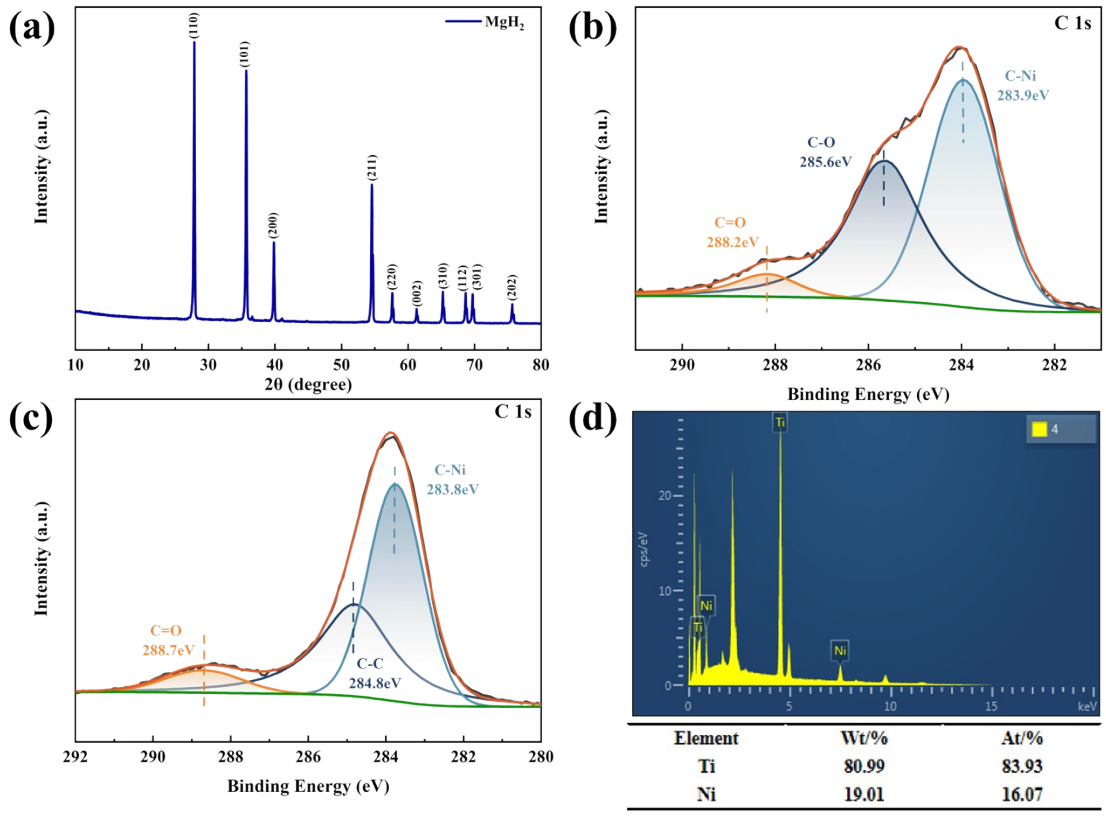

Element	Wt/%	At/%
Ti	80.99	83.93
Ni	19.01	16.07

Fig. S1. (a) XRD pattern of the original MgH_2; XPS spectra of C in (b) Ti_4Ni and (c) MgH_2-$CTi_4Ni@CNT_1$; (d) EDS of Ti_4Ni

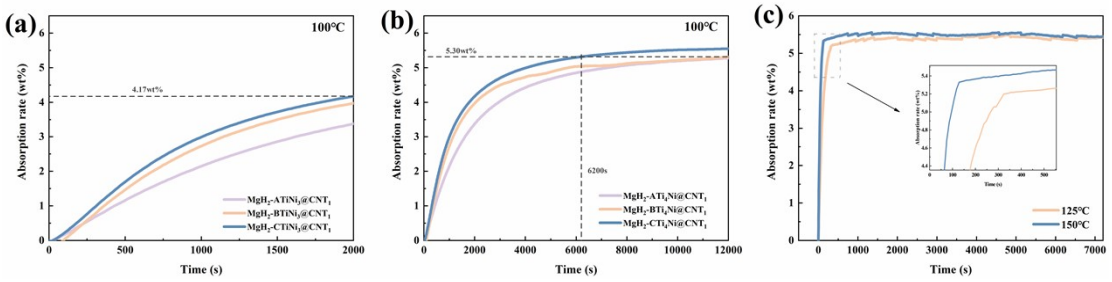

Fig. S2. Isothermal hydrogen absorption curves of MgH_2-$Ti_4Ni@CNT_1$ at 100 °C for part (a) and whole (b); (c) isothermal hydrogen absorption curves of MgH_2-$Ti_4Ni@CNT_1$ at 100 and 150 °C.

It should be noted that in Fig. S2c, the curve of hydrogen absorption in the later stage is a normal fluctuation phenomenon, which does not affect the MgH_2-$CTi_4Ni@CNT_1$ The judgment of hydrogen storage performance and the subsequent dynamic fitting calculation process.

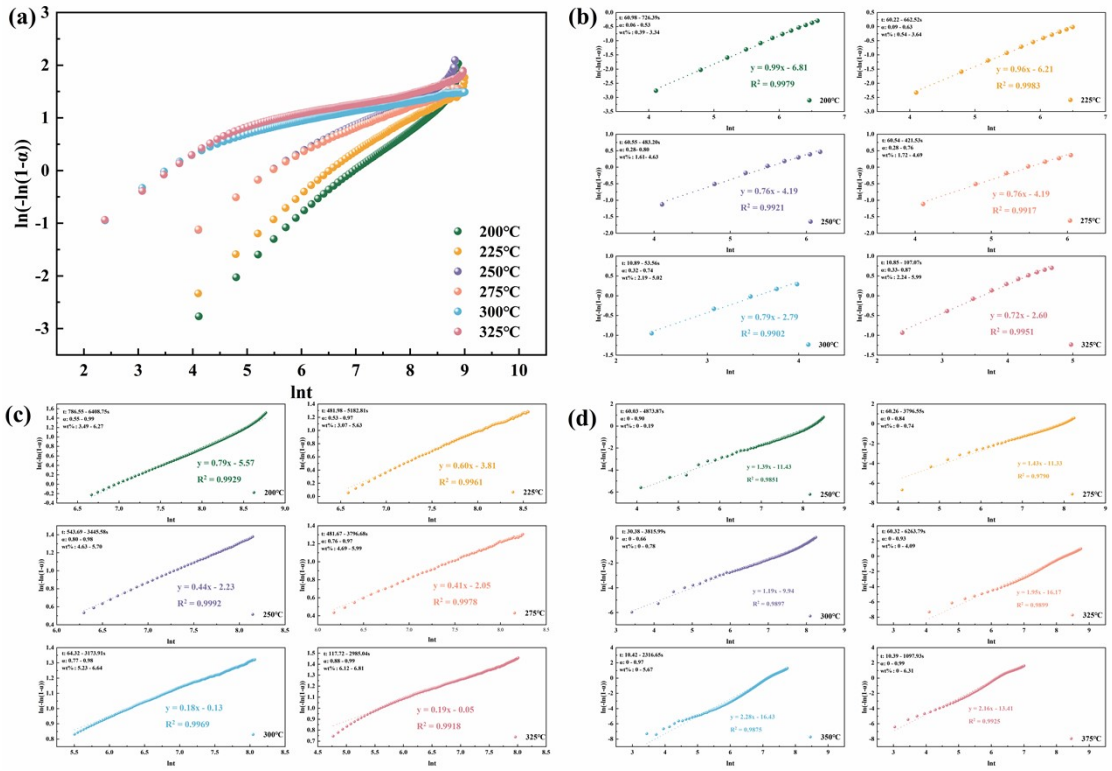

Fig. S3. The JMAK fitting plots of BM-MgH_2: (a) overall hydrogenation, (b) early hydrogenation, (c) late hydrogenation, and (d) dehydrogenation.

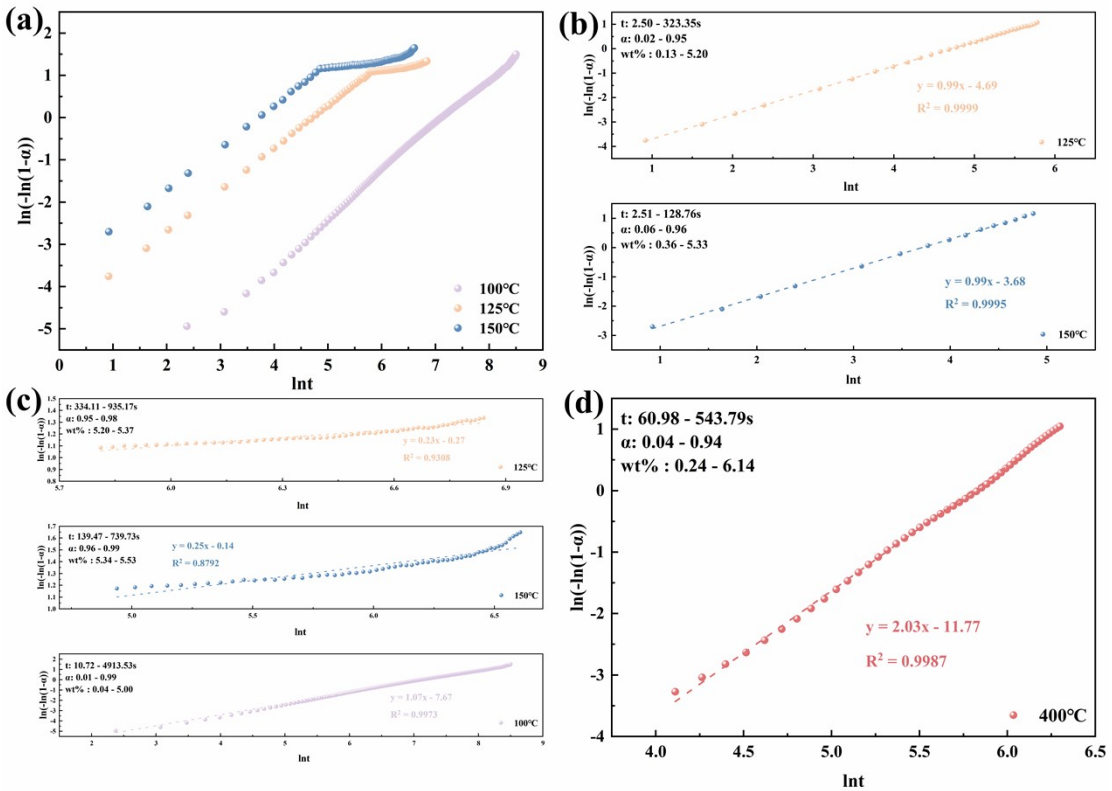

Fig. S4. JMAK fitting plots of MgH_2-CTi_4Ni@CNT_1 at 100, 125 and 150°C: (a) overall hydrogenation, (b) early hydrogenation, (c) late hydrogenation; (d) JMAK fitting plots of BM-

MgH_2 at 400 °C.

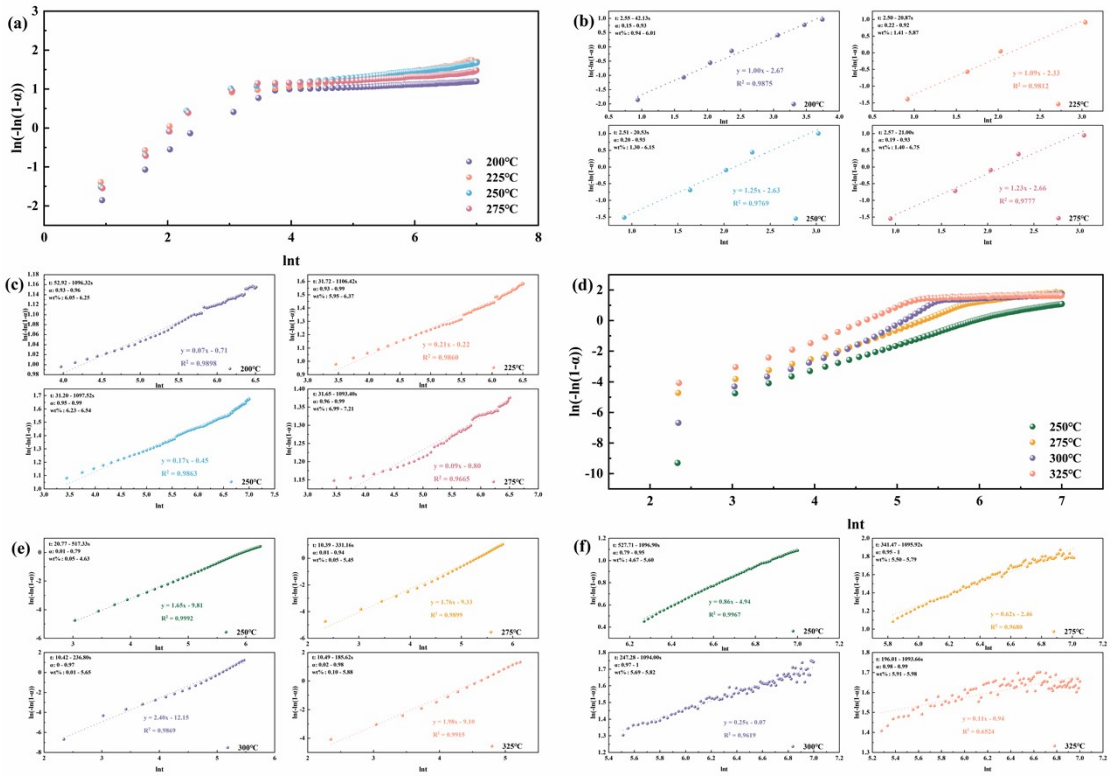

Fig. S5. JMAK fitting plots of MgH_2-CTi_4Ni@CNT_1: (a) overall hydrogenation, (b) early hydrogenation, (c) late hydrogenation, (d) overall dehydrogenation, (e) early dehydrogenation, (f) late dehydrogenation.

The fitting results shown in Figs. S3, S4, and S5 reveal a common trend for both MgH_2-CTi_4Ni@CNT_1 and BM-MgH_2: the segmented characteristics of the JMAK curves become increasingly pronounced with increasing temperature. This indicates that the hydrogen absorption and desorption processes of both samples are not governed by a single kinetic step, but rather consist of multiple reaction processes.

Based on this feature, a segmented fitting method was adopted in this work to extract the ln$k$ values for activation-energy calculation, instead of treating the data uniformly on the basis of the overall reaction fraction α. The purpose of this treatment is to ensure, as far as possible, that the selected fitting interval at a given temperature corresponds to a relatively consistent overall rate-controlling regime, thereby making the activation-energy analysis more physically meaningful.

However, the increase in temperature only enhances the separation of different rate-controlling steps to a certain extent, and does not imply that the kinetic parameters extracted at different temperatures correspond to exactly the same single reaction process. In other words, the relative contributions of the individual subprocesses to the overall macroscopic reaction vary with temperature, and therefore

the ln*k* values obtained at different temperatures do not strictly correspond to the same kinetic "object". This is also the main reason why the R^2 values of the activation-energy fitting could not be guaranteed to exceed 0.99.

Therefore, the activation energies obtained in this work are more appropriately interpreted as apparent activation energies, rather than the intrinsic activation energy of a single elementary reaction step. This treatment provides a more reasonable description of the overall kinetic characteristics of hydrogen absorption and desorption in complex systems such as MgH_2-CTi_4Ni@CNT_1 and BM-MgH_2.

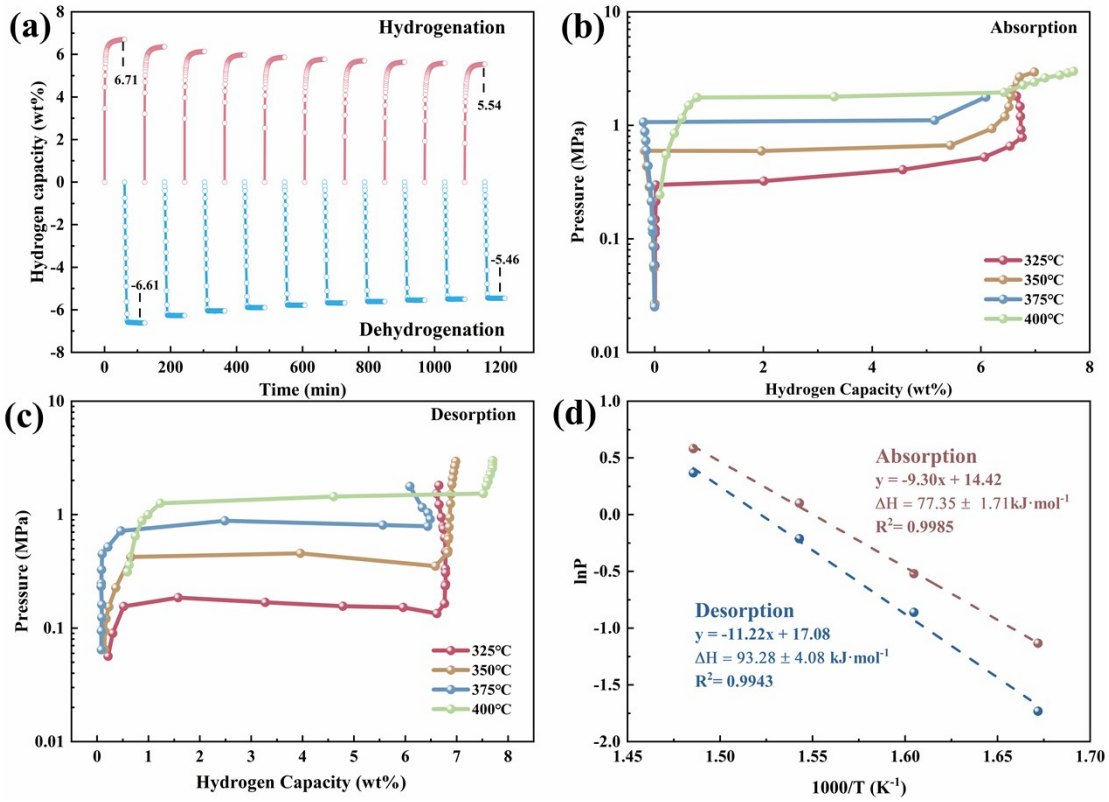

Fig. S6. (a) Cycle test curve of Ball milled MgH_2; PCT test curve of BM-MgH_2 by (b) hydrogenation and (c) dehydrogenation; (d) Fit results of BM-MgH_2 by van't Hoff equation.

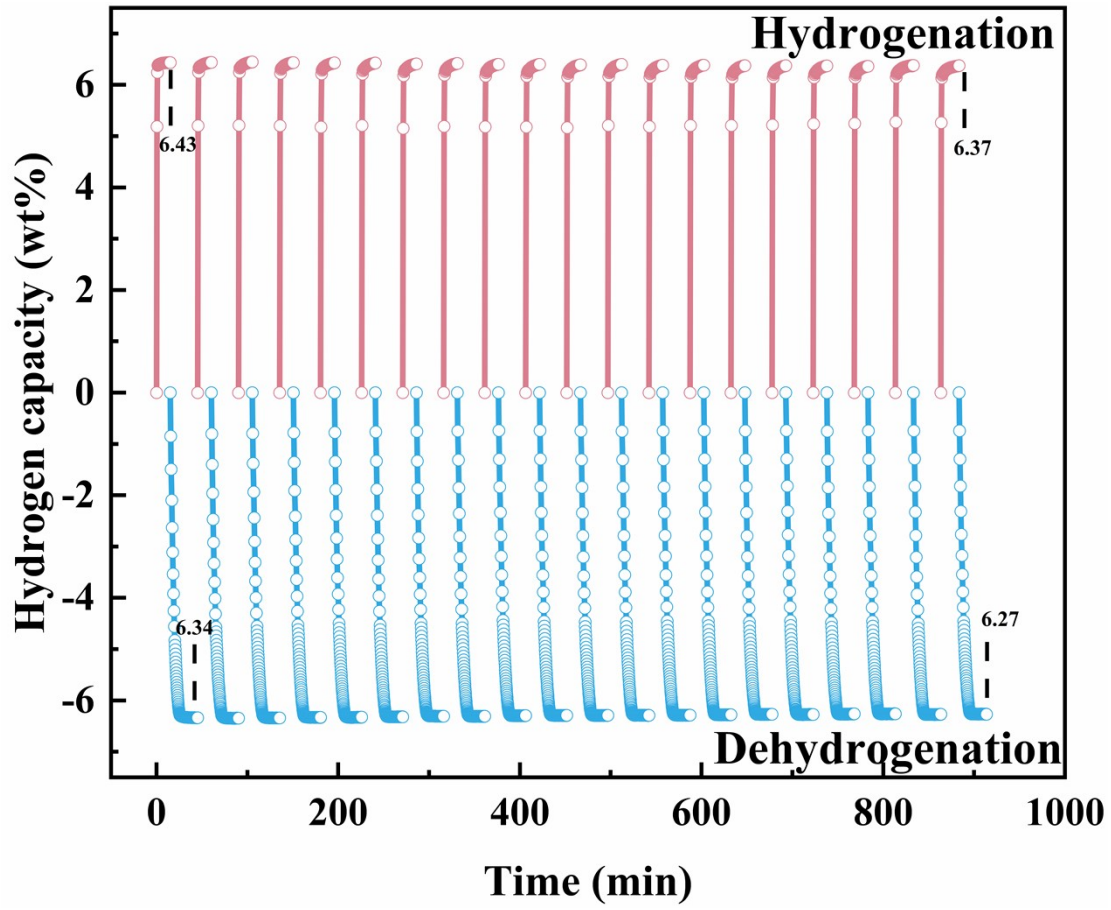

Fig. S7. Cyclic results of MgH_2-CTi_4Ni@CNT_1 after compaction.

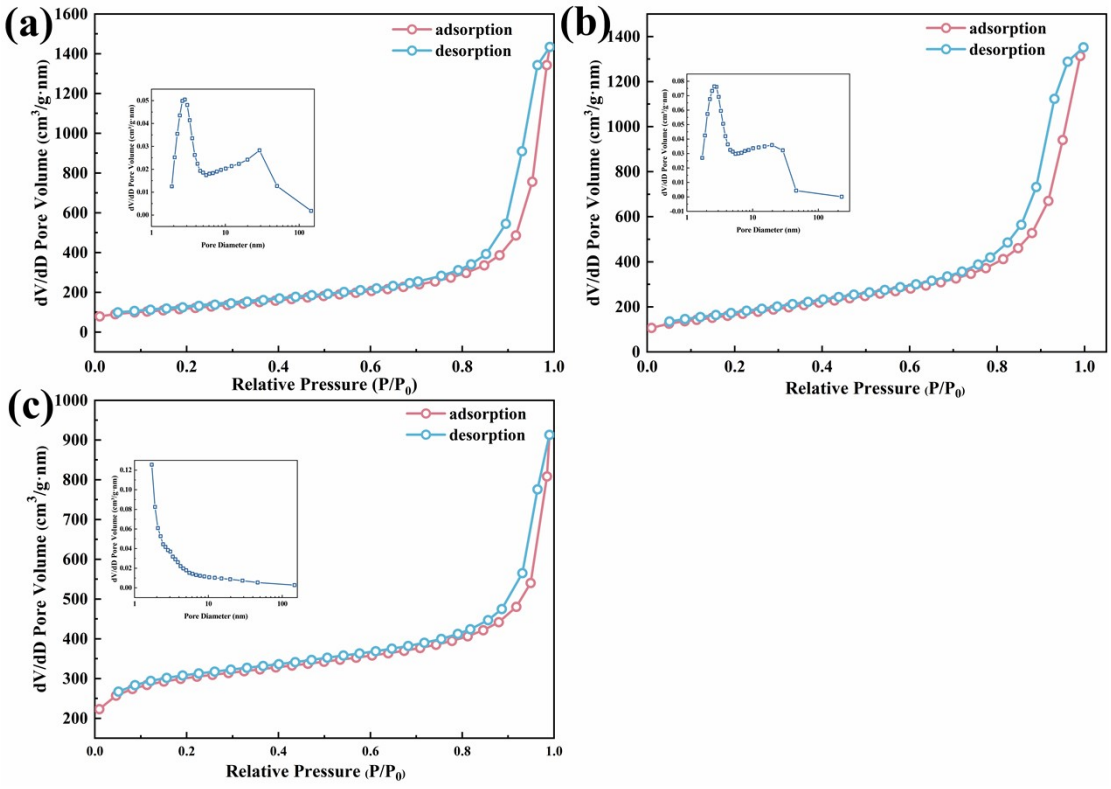

Fig. S8. BET specific surface area and pore size test results of (a) CNT_1, (b) CNT_2 and (c) CNT_3.

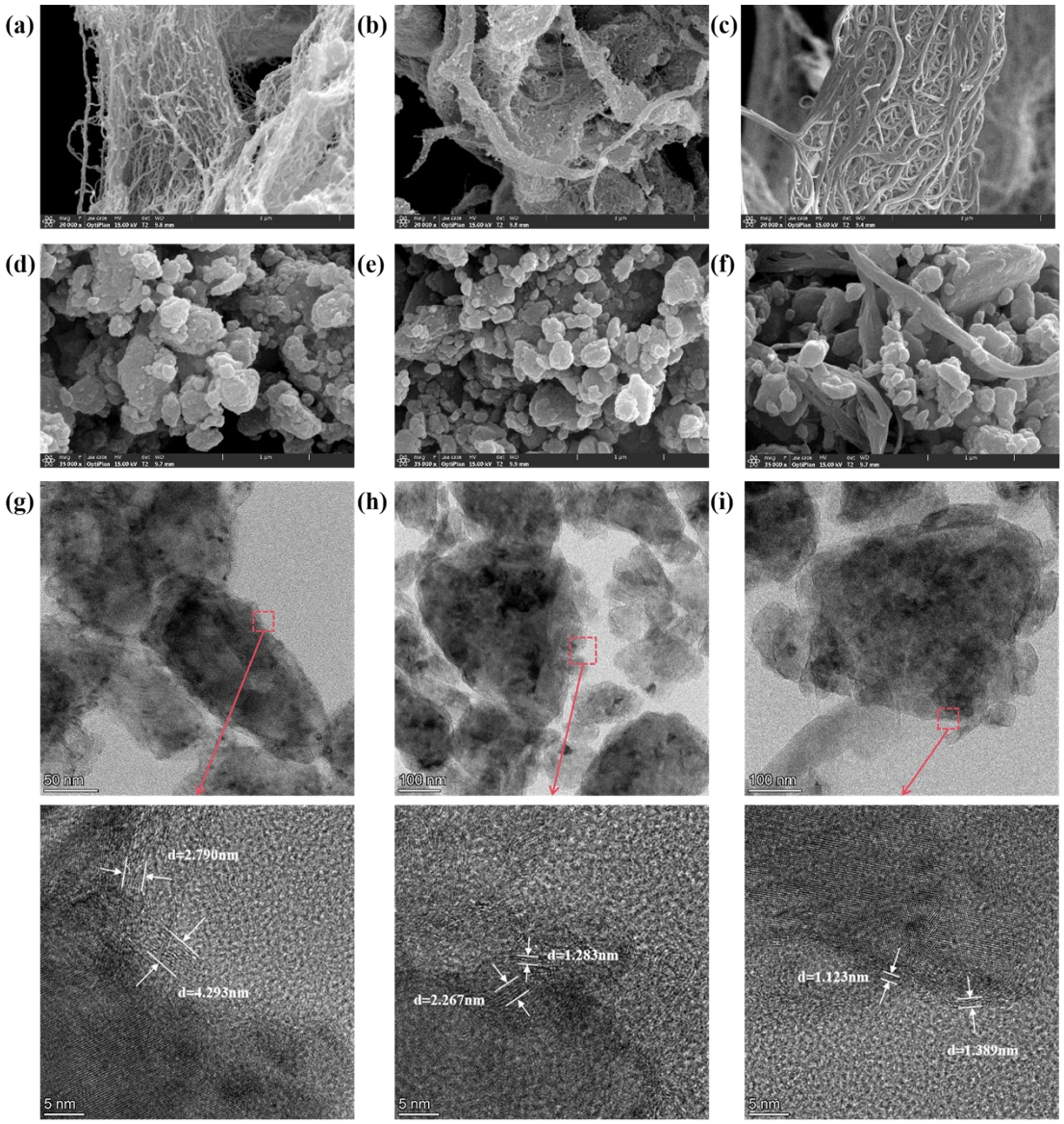

Fig. S9. SEM images of (a) CNT_1, (b) CNT_2, (c) CNT_3, (d) MgH_2-5wt% CNT_1, (e) MgH_2-5wt% CNT_2 and (f) MgH_2-5wt% CNT_3; TEM and HRTEM images of (g) MgH_2-5wt% CNT_1, (h) MgH_2-5wt% CNT_2 and (i) MgH_2-5wt% CNT_3.

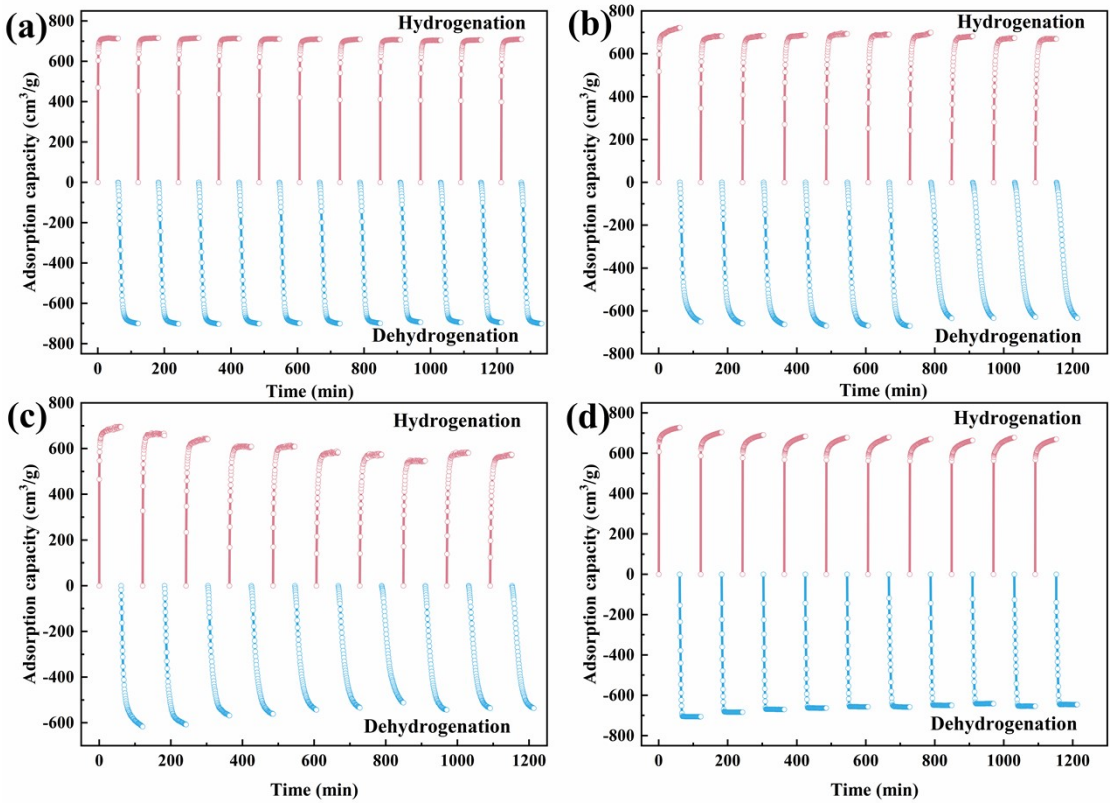

Fig. S10. Cycle test data of (a) MgH_2-5wt%CNT_1, (b) MgH_2-5wt%CNT_2, (c) MgH_2-5wt%CNT_3 and (d) MgH_2-7.5wt%Ti_4Ni.

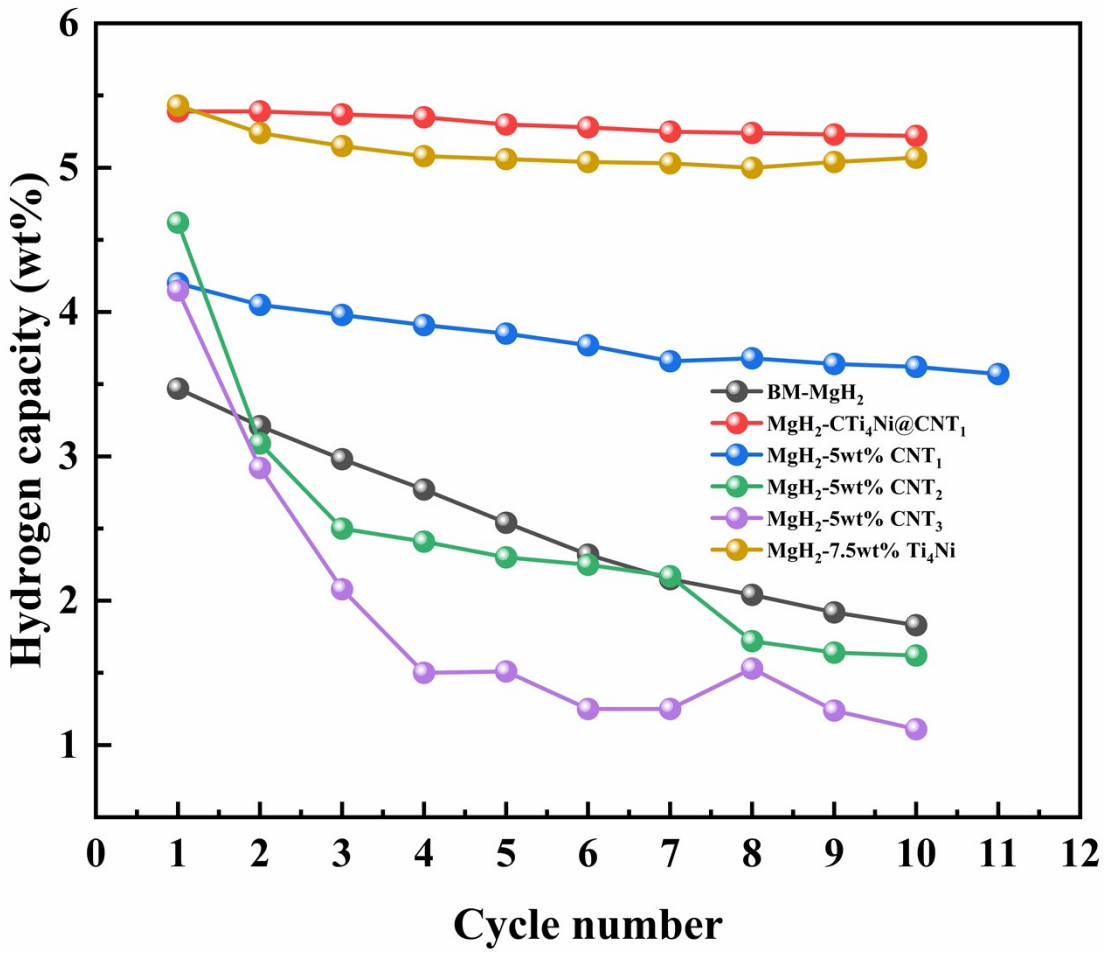

Fig. S11. Comparison of hydrogen absorption changes in the first 30 seconds of cyclic testing.

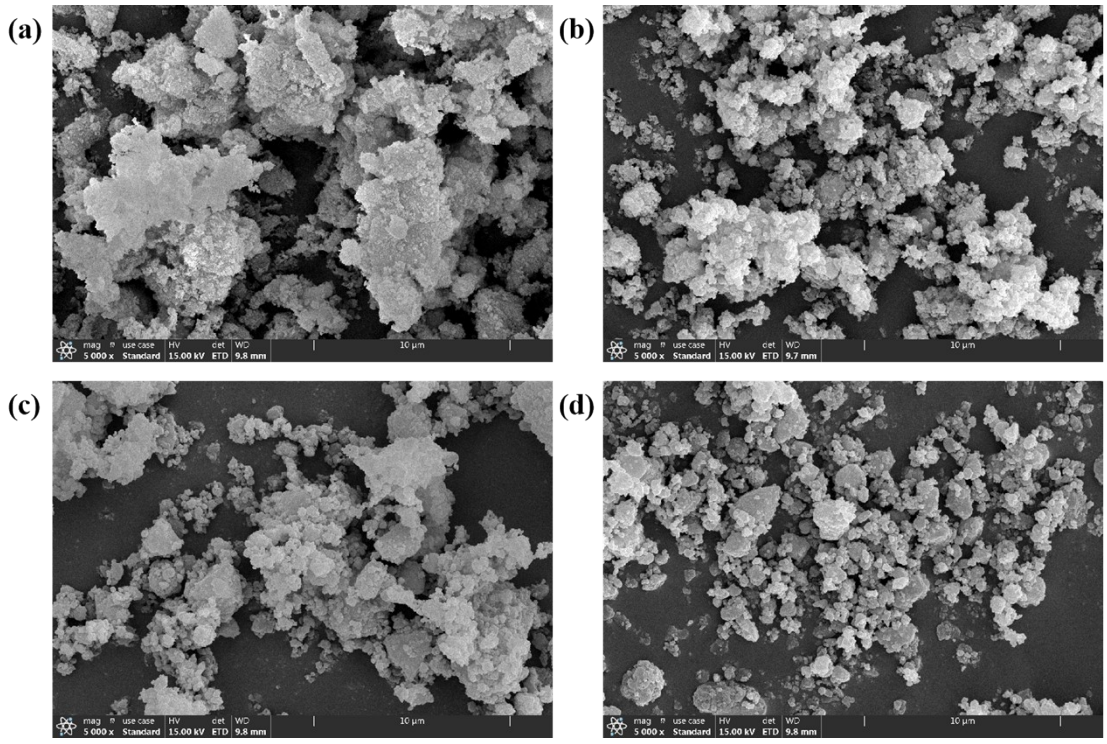

Fig. S12. SEM images of (a) BM-MgH_2 after cycling, (b) MgH_2-CTi_4Ni@CNT_1 after cycling, (c) BM-MgH_2 before cycling, and (d) MgH_2-CTi_4Ni@CNT_1 before cycling.

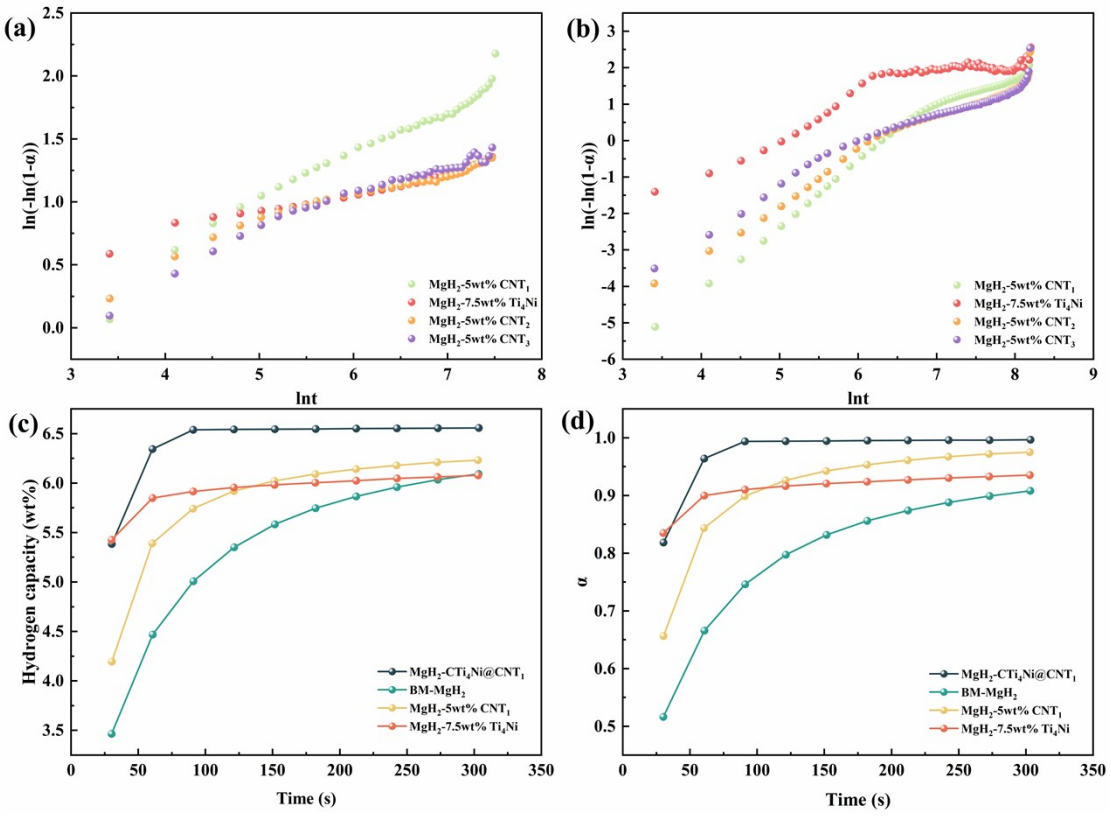

Fig S13. JMAK of MgH_2-5wt%CNT_1, MgH_2-5wt%CNT_2, MgH_2-5wt%CNT_3 and MgH_2-7.5wt%Ti_4Ni: (a) hydrogen absorption, (b) hydrogen desorption; (c) hydrogen absorption capacity and (d) reaction progress of BM-MgH_2, MgH_2-CTi_4Ni@CNT_1, MgH_2-5wt%CNT_1 and MgH_2-

7.5wt%Ti_4Ni.

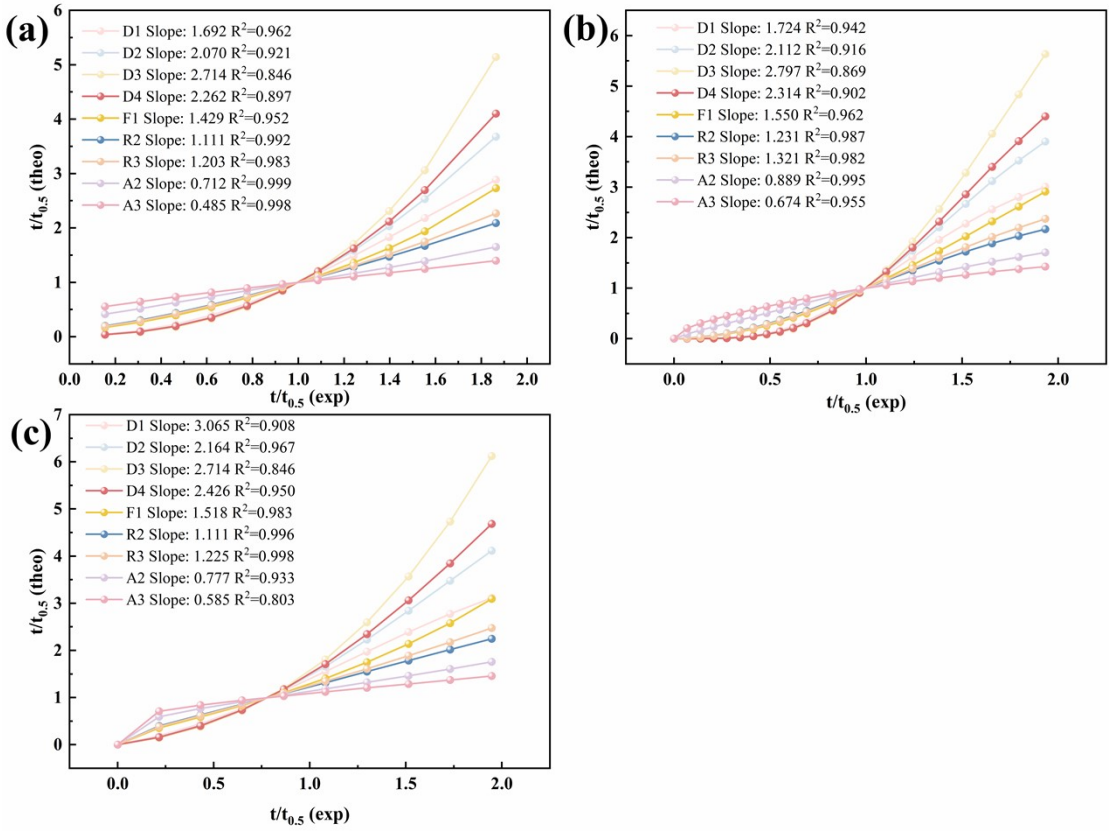

Fig. S14. Comparison of $t/t_{0.5}$ (theo) and $t/t_{0.5}$ (exp) for isothermal dehydrogenation of (a) BM-MgH_2, (b) MgH_2-5wt%CNT_1 and (c) MgH_2-7.5wt%Ti_4Ni.

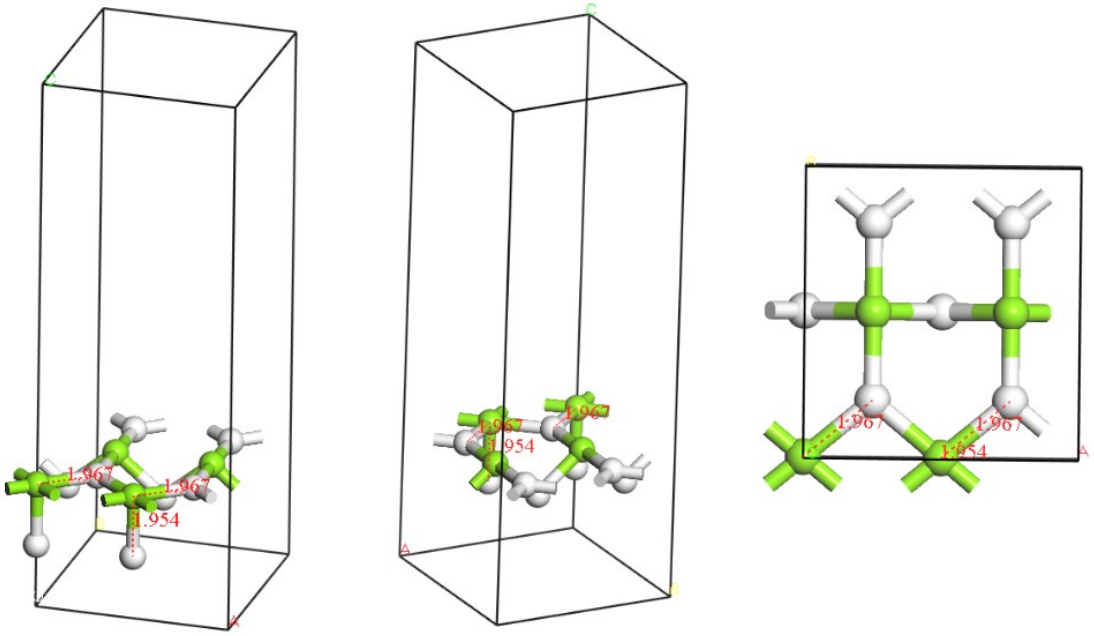

Fig. S15. Sectional model of pure MgH_2 on the (1 1 0) plane. (green: Mg, white: H)

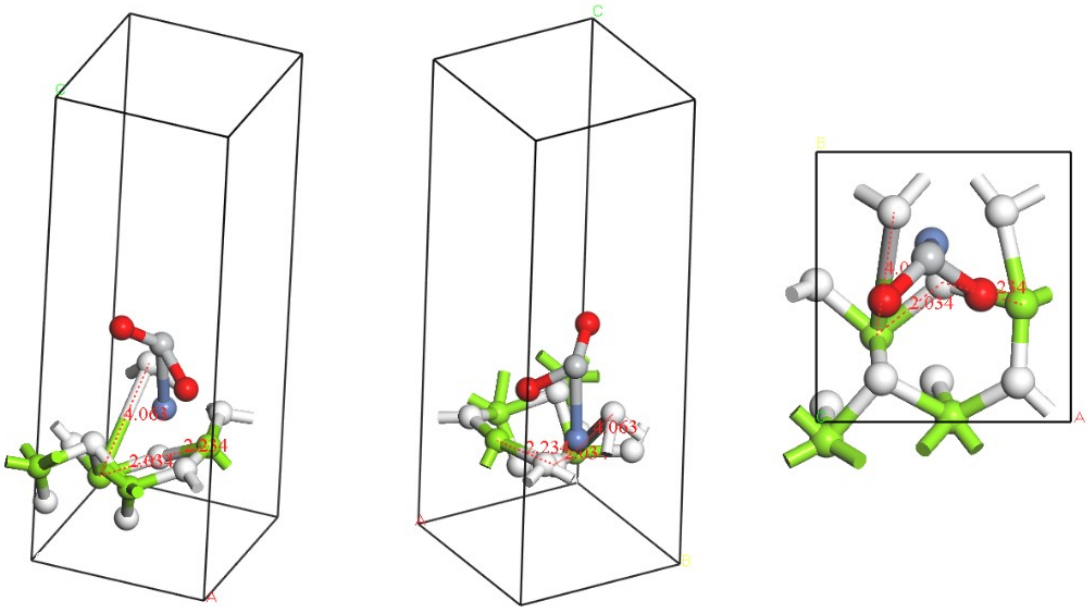

Fig. S16. Sectional model of MgH_2 doped with Ti_4Ni on the (1 10) plane. (green: Mg, white: H, blue: Ni, gray: Ti, red: O)

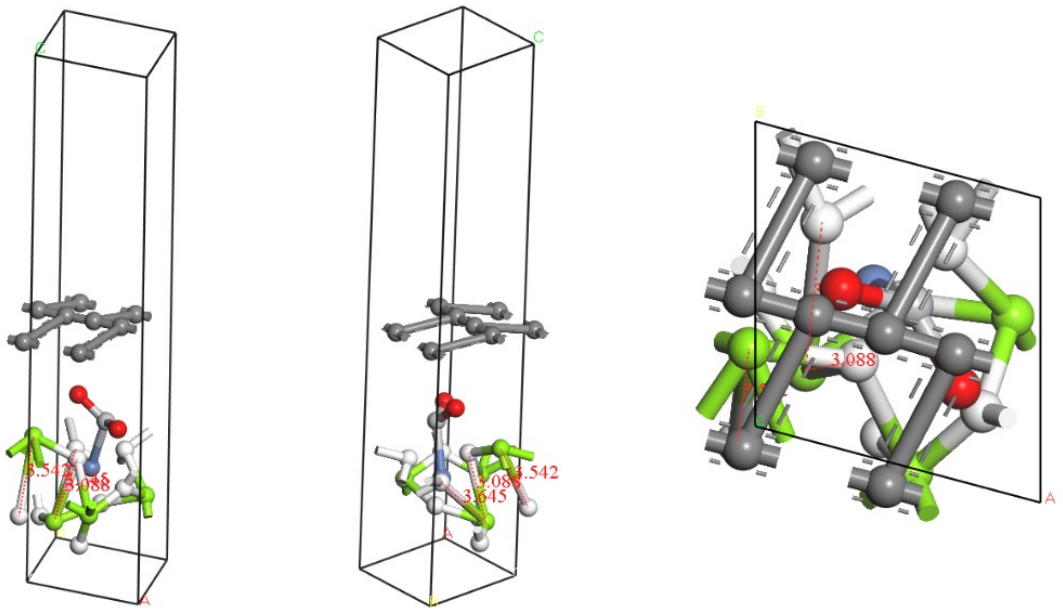

Fig. S17. Sectional model of MgH_2 doped with Ti_4Ni and CNT_1 on the (1 1 0) plane. (green: Mg, white: H, blue: Ni, gray: Ti, red: O, black: C)

The introduction of a vacuum layer is to avoid the influence of periodic repetitive structures. Due to the sufficient thickness of the vacuum layer, the impact on the calculation of electronic properties can be ignored.

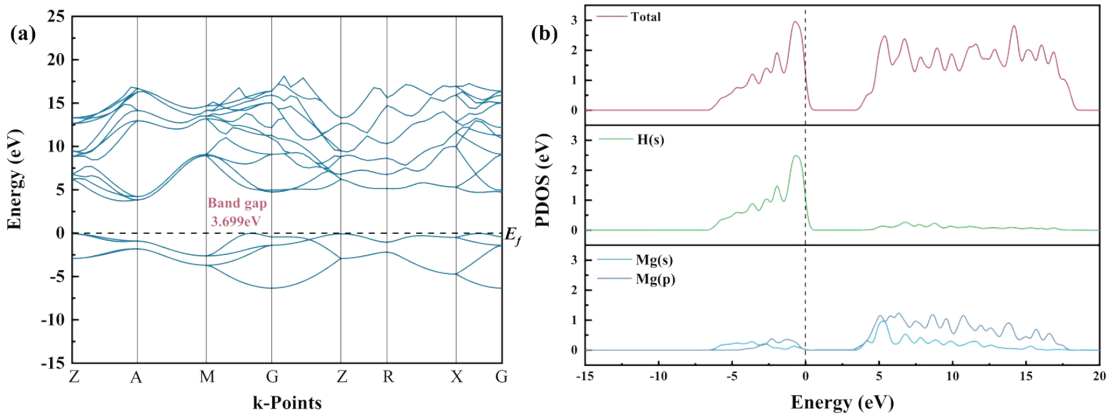

Fig. S18. (a) Band structure and (b) density of states of MgH_2 (1 1 0) section.

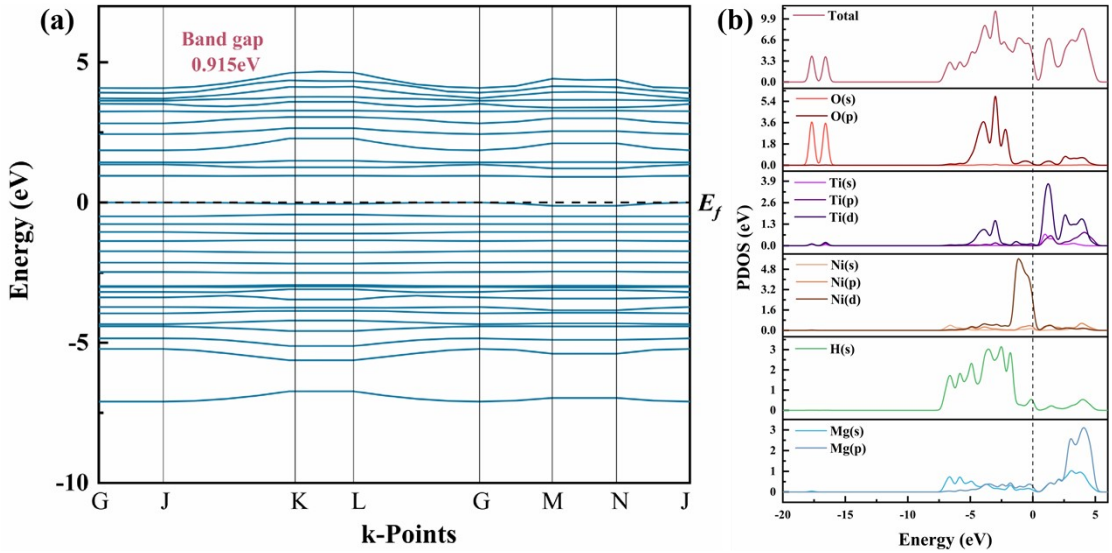

Fig. S19. (a) Band structure and (b) density of states of MgH_2 (1 1 0) section doped with Ti_4Ni.

Table S1 ln*k* value in activation energy calculation

		Temperature (°C)	1000/T (K^{-1})	ln*k*
MgH_2-CTi_4Ni@CNT_1	Hydrogenation	100	2.68	-7.17
		125	2.51	-4.74
		150	2.36	-3.72
		200	2.11	-2.67
		225	2.01	-2.13
		250	1.91	-2.11
		275	1.82	-2.16
	Dehydrogenation	250	1.91	-5.95
		275	1.82	-5.29
		300	1.74	-5.06
		325	1.67	-4.59

BM-MgH_2	Hydrogenation	200	2.11	-6.83
		225	2.01	-6.47
		250	1.91	-5.49
		325	1.67	-3.61
	Dehydrogenation	250	1.91	-8.20
		275	1.82	-7.91
		300	1.74	-8.38
		325	1.67	-8.29
		350	1.60	-7.19
		375	1.54	-6.21
		400	1.49	-5.80

Table S2 Plateau pressures

Reaction process	Materials	Temperature (℃)	Plateau pressures (MPa)
Hydrogen absorption	BM-MgH_2	325	0.322
		350	0.595
		375	1.108
		400	1.792
	MgH_2-CTi_4Ni@CNT_1	325	0.632
		350	0.843
		375	1.106
		400	1.400
Hydrogen desorption	BM-MgH_2	325	0.177
		350	0.423
		375	0.809
		400	1.446
	MgH_2-CTi_4Ni@CNT_1	325	0.491
		350	0.663
		375	0.935
		400	1.257

During the PCT testing process, pressure can vary. Therefore, when selecting the platform pressure for fitting, it is usually necessary to take the average of at least two consecutive data points, and the pressure difference between these two data points should not exceed 0.05 MPa. If multiple consecutive data points meet this requirement, then the average of these data points should be taken.

Table S3 Detailed data of three types of carbon nanotubes

Materials	Specific surface areas ($m^2 \cdot g^{-1}$)	Pore size (nm)	Type of pore	Thickness (nm)

CNT_1	400	2 - 20	mesoporous	2.7 - 4.3
CNT_2	600	2 - 10	mesoporous	1.2 - 2.3
CNT_3	1100	< 5	microporous	1.1 - 1.4

Table S4 Detailed comparison of cyclic performance data

Materials	Adsorption capacity (wt%)		Desorption capacity (wt%)		Adsorption capacity (cm^3/g)		Desorption capacity (cm^3/g)		Cycle capacity retention rate (%)		Adsorption capacity within the first 30s (wt%)
	1st	10th	1st	10th	1st	10th	1st	10th	Adsorption	Desorption	
MgH_2-CTi_4Ni@CNT_1	6.58	6.49	6.42	6.36	736.8	727.5	719.1	712.0	98.6	99.1	5.39
BM-MgH_2	6.71	5.54	6.61	5.46	751.5	620.7	740.9	611.2	82.6	82.6	3.47
MgH_2-5wt%CNT_1	6.37	6.34	6.25	6.25	713.8	700.0	709.7	699.8	98.1	98.6	4.20
MgH_2-5wt%CNT_2	6.44	5.97	5.81	5.66	721.7	669.0	651.3	633.8	92.7	97.3	4.62
MgH_2-5wt%CNT_3	6.20	5.12	5.50	4.79	694.6	573.3	616.2	536.4	82.5	87.0	4.15
MgH_2-7.5wt%Ti_4Ni	6.50	5.98	6.31	5.77	728.1	670.1	706.2	646.1	92.0	91.5	5.43
MgH_2-CTi_4Ni@CNT_1 after compaction	1st	20th	1st	20th	1st	20th	1st	20th	99.1	98.9	5.19
	6.43	6.37	6.34	6.27	720.7	713.8	709.6	702.1			

Table S5 Grain size calculated based on the (101) crystal plane

Materials	Grain size (nm)
Dehydrogenation	79.23
Dehydrogenation (10th cycle)	83.64

XRD results was used to calculated grain size, combined with Scherrer formula:

$$D = K\lambda / \beta cos\theta \quad (1)$$

D is the grain size (nm), K is the Scherrer constant 0.89, λ is the X-ray incident wavelength (nm), B is the diffraction peak broadening amount (rad), and θ is the Bragg angle (rad).